Effect of Secondary Structure on the Thermodynamics and Kinetics of PNA Hybridization to DNA Hairpins

Stuart A. Kushon, Jason P. Jordan, Jennifer L. Seifert, Henrik Nielsen,[†] Peter E. Nielsen,[‡] and Bruce A. Armitage*

Contribution from the Department of Chemistry, Carnegie Mellon University, 4400 Fifth Avenue, Pittsburgh, Pennsylvania 15213-3890

Received May 30, 2001

Abstract: The binding of a series of PNA and DNA probes to a group of unusually stable DNA hairpins of the tetraloop motif has been observed using absorbance hypochromicity (ABS), circular dichroism (CD), and a colorimetric assay for PNA/DNA duplex detection. These results indicate that both stable PNA−DNA and DNA−DNA duplexes can be formed with these target hairpins, even when the melting temperatures for the resulting duplexes are up to 50 °C lower than that of the hairpin target. Both hairpin/single-stranded and hairpin/hairpin interactions are considered in the scope of these studies. Secondary structures in both target and probe molecules are shown to depress the melting temperatures and free energies of the probe−target duplexes. Kinetic analysis of hybridization yields reaction rates that are up to 160-fold slower than hybridization between two unstructured strands. The thermodynamic and kinetic obstacles to hybridization imposed by both target and probe secondary structure are significant concerns for the continued development of antisense agents and especially diagnostic probes.

Introduction

The ability of an oligonucleotide to recognize a complementary sequence of a natural DNA or RNA strand according to the Watson−Crick rules for base pairing has led to widespread applications in research, medicine, and diagnostics, and antisense oligonucleotides are now being developed as therapeutic agents for human disease.[1−5] Oligonucleotide hybridization is also being used both commercially and experimentally in diagnostics such as real-time detection of polymerase chain reaction (PCR) products and for identifying disease-related genes and pathogens.[6] A serious consideration in the practical application of hybridization probes is the ubiquity of secondary (2°) and tertiary (3°) folding interactions found in biologically relevant DNA and RNA targets.[7−12] The secondary and tertiary structure present in biological nucleic acids stabilizes the three-dimensional structures required for both cellular recognition and biocatalysis.[10,13,14] In many cases of reaction catalysis by nucleic acids, the secondary and tertiary structures allow the formation of a binding pocket that enables catalysis. The selective disruption of the critical secondary and tertiary structures could disturb the formation of the binding pocket and molecular recognition.[15] Another method of regulating nucleic acid function is the antisense method, where a site-specific hybridization agent is bound to a messenger RNA (mRNA) with the goal of preventing translation of the mRNA by the ribosome. In most cases studied so far, this is accomplished via an Rnase H dependent mechanism using phosphorothioate oligonucleotides,[16,17] but a large variety of oligonucleotide analogues and mimics are now also in development.[18−20]

Structured targets have been shown to influence the stability of probe−target hybrids.[21] Studies have considered the effect of single-stranded structure on the thermodynamics of duplex formation where the self-structure was weak enough to be completely destabilized at the temperatures of duplex dissociation.[22,23] Thus, while the secondary structure was found to reduce the free energy of hybridization, there was no impact on the thermal stability (T_m) of the hybrid. Few reports have quanti-

* E-mail: army@cyrus.andrew.cmu.edu.

[†] Department of Medical Biochemistry and Genetics, Panum Institute, University of Copenhagen, DK 2200 Copenhagen N, Denmark.

[‡] Center for Biomolecular Recognition, IMBG, Department B, Panum Institute, University of Copenhagen, Blegdamsvej 3c 2200 Copenhagen N, Denmark.

(1) Agrawal, S.; Kandimalla, E. R. *Mol. Medicine Today* **2000**, *6*, 72−81.

(2) Juliano, R. L.; Alahari, S.; Yoo, H.; Kole, R.; Cho, M. *Pharm. Res.* **1999**, *16*, 494−502.

(3) Marcusson, E. G.; Yacyshyn, B. R.; Shanahan, W. R.; Dean, N. M. *Mol. Biotechnol.* **1999**, *12*, 1−11.

(4) Nielsen, P. E. *Curr. Opin. Struct. Biol.* **1999**, *9*, 353−357.

(5) Bennett, C. F. *Biochem. Pharmacol.* **1998**, *55*, 9−19.

(6) Cotton, R. G. *Mutat. Res.* **1993**, *285*, 125.

(7) Tuerk, C.; al, e. *Proc. Natl. Acad. Sci. U.S.A.* **1988**, *85*, 1364−1368.

(8) Klausner, R. D.; Rouault, T. A. *Cell* **1993**, *72*, 19−28.

(9) Varani, G. *Annu. Rev. Biophys. Biomol. Struct.* **1995**, *24*, 379−404.

(10) Lehnert, V.; Jaeger, L.; Michel, F.; Westhof, E. *Chem. Biol.* **1996**, *3*, 993−1009.

(11) Dai, X.; Greizerstein, M. B.; Nadas-Chinni, K.; Rothman-Denes, L. B. *Proc. Natl. Acad. Sci. U.S.A.* **1997**, *94*, 2174−2179.

(12) Dai, X.; Kloster, M.; Rothman-Denes, L. B. *J. Mol. Biol.* **1998**, *283*, 43−58.

(13) Batey, R. T.; Rambo, R. P.; Doudna, J. A. *Angew. Chem., Int. Ed. Engl.* **1999**, *38*, 2326−2343.

(14) Belmont, P.; Constant, J.-F.; Demeunynck, M. *Chem. Soc. Rev.* **2001**, *30*, 70−81.

(15) Wilson, D. S.; Szostak, J. W. *Annu. Rev. Biochem.* **1999**, *68*, 611−647.

(16) Crooke, S. T. *Biochim. Biophys. Acta* **1999**, *1489*, 31−44.

(17) Giles, R. V.; Tidd, D. M. *Methods Mol. Biol.* **2001**, *160*, 157−182.

(18) De Mesmaeker, A.; Haener, R.; Martin, P.; Moser, H. E. *Acc. Chem. Res.* **1995**, *28*, 366−374.

(19) Nielsen, P. E. *Curr. Opin. Mol. Ther.* **2000**, *2*, 282−287.

(20) Braasch, D. A.; Corey, D. R. *Chem. Biol.* **2001**, *8*, 1−7.

(21) Ørum, H.; Nielsen, P. E.; Jørgensen, M.; Larsson, C.; Stanley, C.; Koch, T. *BioTechniques* **1995**, *19*, 472−480.

(22) Vesnaver, G.; Breslauer, K. J. *Proc. Natl. Acad. Sci. U.S.A.* **1991**, *88*, 3569−3573.

(23) Armitage, B.; Ly, D.; Koch, T.; Frydenlund, H.; Ørum, H.; Schuster, G. B. *Biochemistry* **1998**, *37*, 9417−9425.

10.1021/ja016310e CCC: $20.00
Published on Web 10/13/2001

tatively considered the effects of secondary structure on probe hybridization.[24,25] Our goal is to analyze the thermodynamics and kinetics for binding of hybridization probes to simple oligonucleotides that fold into stable secondary structures. In particular, the hairpin motif is an excellent choice for thermodynamic study because of the experimentally controllable thermal and thermodynamic stabilities and the array of biological function displayed by members of this class of structures. A variety of DNA and RNA hairpins have been found to exhibit extraordinary stability.[26−30] These structures should be difficult to overcome because of this stability, and thus hairpin targets should serve as a rigorous test of any hybridization probe. Furthermore, hairpins are the dominant secondary structural motif in RNA.[9] Among other important roles, RNA hairpins determine nucleation sites for folding,[7] define the three-dimensional structures of ribozymes through tertiary interactions (i.e., loop/loop and loop/bulge interactions),[10] and regulate mRNA degradation.[8] DNA hairpins have also been proposed to be protein recognition sites,[11] and hairpin extrusion mechanisms have been suggested in pathways of viral replication.[12]

Peptide nucleic acid (PNA) is a DNA mimic where the phosphodiester-linked backbone has been replaced with an *N*-(2-aminoethyl)glycine backbone.[31−33] PNA binds to complementary single-stranded targets according to the Watson−Crick rules for base pairing, and for most sequences, PNA binds its DNA targets with higher affinity than DNA binds to the same targets.[34] This high affinity comes partially as a result of the neutral character of the PNA backbone, which alleviates the standard charge−charge repulsion of duplex formation. More importantly, the mismatch discrimination of PNA is in many cases better than that of DNA, and so PNA is not only a high affinity probe for DNA, but it also maintains high specificity.[34−36] In some cases, the high affinity of PNA (especially for triplex forming homopyrimidine PNAs) even permits hybridization to duplex DNA targets via "strand invasion",[31,37−45] suggesting that PNA could potentially overcome nonduplex secondary and tertiary structures as well. The advantages exhibited by PNA over DNA probes have led to its use in a variety of biological applications, including inhibition of human telomerase,[46−51] capture of nucleic acids for purification,[21,52] and inhibition of gene expression in cell culture.[19,53,54]

It is well established that only a small subset of all possible sequence targets on a given mRNA is sensitive to antisense inhibition.[55a] Many factors influence this sensitivity, and structural accessibility of the target is undoubtedly an important parameter. Accordingly, Corey and co-workers reported antisense studies on a group of 27 PNAs that were targeted to the 5′-untranslated region, start site, and coding regions of the luciferase mRNA with the intent to inhibit gene expression. Only the PNAs directed toward the terminal portion of the 5′-untranslated region effectively blocked gene expression.[55b]

In this paper, we quantify the thermodynamic and kinetic impact of a simple DNA secondary structure, the hairpin, on PNA hybridization. We also provide data for corresponding DNA probes for comparison and consider further cases where both the probe and target adopt stable secondary structures. The results of these studies should assist in beginning to define criteria for the rational design of hybridization probes and possibly antisense agents.

Experimental Section

Chemicals. DNA oligonucleotides (purified by gel filtration chromatography) were purchased from Integrated DNA Technologies, Inc., (http://www.idtdna.com) and were used without further purification. One oligonucleotide purified by polyacrylamide gel electrophoresis yielded the same results as a GF grade oligonucleotide in these experiments. Literature values for DNA extinction coefficients were obtained and used as stated.[56] Concentration determinations were based on absorption at 260 nm and were measured at 80 °C on a Cary 3 Bio spectrophotometer. At 80 °C, the nucleobases are assumed to be completely unstacked, and the absorptivity is then assumed to be the sum of the absorptivities of the DNA monomers. DNA concentrations were also confirmed by chemical degradation followed by phosphorus analysis.[57] PNA monomers were purchased from PE

(24) Gregorian, R. S.; Crothers, D. M. *J. Mol. Biol.* **1995**, *248*, 968−984.
(25) Bonnet, G.; Tyagi, S.; Libchaber, A.; Kramer, F. R. *Proc. Natl. Acad. Sci. U.S.A.* **1999**, *96*, 6171−6176.
(26) Hirao, I.; Nishimura, Y.; Naraoka, T.; Watanabe, K.; Arata, Y.; Miura, K.-i. *Nucleic Acids Res.* **1989**, *17*, 2223−2231.
(27) Antao, V. P.; Lai, S. Y.; Tinoco, I. J. *Nucleic Acids Res.* **1991**, *19*, 5901−5905.
(28) Antao, V. P.; Tinoco, I. J. *Nucleic Acids Res.* **1992**, *20*, 819−824.
(29) Rentzeperis, D.; Alessi, K.; Marky, L. A. *Nucleic Acids Res.* **1993**, *21*, 2683−2689.
(30) Williams, D. J.; Hall, K. B. *Biochemistry* **1996**, *35*, 14665−14670.
(31) Nielsen, P. E.; Egholm, M.; Berg, R. H.; Buchardt, O. *Science* **1991**, *254*, 1498−1500.
(32) Nielsen, P. E.; Haaima, G. *Chem. Soc. Rev.* **1997**, *26*, 73−78.
(33) Ganesh, K. N.; Nielsen, P. E. *Curr. Org. Chem.* **2000**, *4*, 916−928.
(34) (a) Giesen, U.; Kleider, W.; Berding, C.; Geiger, A.; Ørum, H.; Nielsen, P. E. *Nucleic Acids Res.* **1998,** *26*, 5004−5006. (b) Egholm, M.; Buchardt, O.; Christensen, L.; Behrens, C.; Freier, S. M.; Driver, D. A.; Berg, R. H.; Kim, S. K.; Nordén, B.; Nielsen, P. E. *Nature* **1993**, *365*, 566−568.
(35) Ratilainen, T.; Holmén, A.; Tuite, E.; Haaima, G.; Christensen, L.; Nielsen, P. E.; Nordén, B. *Biochemistry* **1998**, *37*, 12331−12342.
(36) Ratilainen, T.; Holmén, A.; Tuite, E.; Nielsen, P. E.; Nordén, B. *Biochemistry* **2000**, *39*, 7781−7791.
(37) Cherny, D. Y.; Belotserkovskii, B. P.; Frank-Kamenetskii, M. D.; Egholm, M.; Buchardt, O.; Berg, R. H.; Nielsen, P. E. *Proc. Natl. Acad. Sci. U.S.A.* **1993**, *90*, 1667−1670.
(38) Demidov, V. V.; Yavnilovich, M. V.; Belotserkovskii, B. P.; Frank-Kamenetskii, M. D.; Nielsen, P. E. *Proc. Natl. Acad. Sci. U.S.A.* **1995**, *92*, 2637−2641.
(39) Egholm, M.; Christensen, L.; Dueholm, K. L.; Buchardt, O.; Coull, J.; Nielsen, P. E. *Nucleic Acids Res.* **1995**, *23*, 217−222.
(40) Griffith, M. C.; Risen, L. M.; Greig, M. J.; Lesnik, E. A.; Sprankle, K. G.; Griffey, R. H.; Kiely, J. S.; Freier, S. M. *J. Am. Chem. Soc.* **1995**, *117*, 831−832.
(41) Nielsen, P. E.; Christensen, L. *J. Am. Chem. Soc.* **1996**, *118*, 2287−2288.
(42) Wittung, P.; Nielsen, P.; Nordén, B. *Biochemistry* **1997**, *36*, 7973−7979.
(43) Kurakin, A.; Larsen, H. J.; Nielsen, P. E. *Chem. Biol.* **1998**, *5*, 81−89.
(44) Ishihara, T.; Corey, D. R. *J. Am. Chem. Soc.* **1999**, *121*, 2012−2020.
(45) Zhang, X.; Ishihara, T.; Corey, D. R. *Nucleic Acids Res.* **2000**, *28*, 3332−3338.
(46) Norton, J. C.; Piatyszek, M. A.; Wright, W. E.; Shay, J. W.; Corey, D. R. *Nat. Biotechnol.* **1996**, *14*, 615−619.
(47) Hamilton, S. E.; Pitts, A. E.; Katipally, R. R.; Jia, X.; Rutter, J. P.; Davies, B. A.; Shay, J. W.; Wright, W. E.; Corey, D. R. *Biochemistry* **1997**, *36*, 11873−11880.
(48) Pitts, A. E.; Corey, D. R. *Proc. Natl. Acad. Sci. U.S.A.* **1998**, *95*, 11549−11554.
(49) Harrison, J. G.; Frier, C.; Laurant, R.; Dennis, R.; Raney, K. D.; Balasubramanian, S. *Bioorg. Med. Chem. Lett.* **1999**, *9*, 1273−1278.
(50) Hamilton, S. E.; Simmons, C. G.; Kathiriya, I. S.; Corey, D. R. *Chem. Biol.* **1999**, *6*, 343−351.
(51) Villa, R.; Folini, M.; Lualdi, S.; Veronese, S.; Daidone, M. G.; Zaffaroni, N. *FEBS Lett.* **2000**, *473*, 241−248.
(52) Boffa, L. C.; Carpaneto, E. M.; Allfrey, V. G. *Proc. Natl. Acad. Sci. U.S.A.* **1995**, *92*, 1901−1905.
(53) Good, L.; Nielsen, P. E. *Nat. Biotechnol.* **1998**, *16*, 355−358.
(54) Mayhood, T.; Kaushik, N.; Pandey, P. K.; Kashanchi, F.; Deng, L. W.; Pandey, V. N. *Biochemistry* **2000**, *39*, 11532−11539.
(55) (a) Monia, B. P.; Johnston, J. F.; Geiger, T.; Muller, M.; Fabbro, D. *Nat. Med. (N.Y.)* **1996** *2*, 668−75. (b) Doyle, D. F.; Braasch, D. A.; Simmons, C. G.; Janowski, B. A.; Corey, D. R. *Biochemistry* **2001**, *40*, 53−64.
(56) Dawson, R. M. C.; Elliott, D. C.; Elliott, W. H.; Jones, K. M. In *Data for Biochemical Research*; Oxford University Press: New York, 1986; pp 103−114.

Chart 1

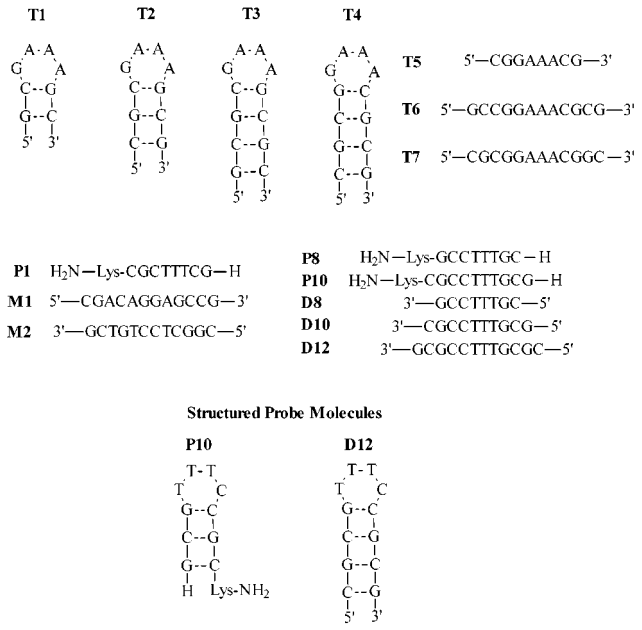

Biosystems (http://www.appliedbiosystems.com) and were used to synthesize PNA probes by a solid-phase peptide synthesis method.[58] PNA probes (Chart 1) were purified via HPLC and characterized by MALDI-TOF mass spectrometry (**P1**: *m*/*z* calculated, 2282.3; found, 2283.9. **P8**: *m*/*z* calculated, 2282.3; found, 2285.0. **P10**: *m*/*z* calculated, 2824.8; found, 2828.0.). Extinction coefficients for PNA monomers were obtained from PE Biosystems (C = 6,600 M^{-1} cm^{-1}; T = 8,600 M^{-1} cm^{-1}; A = 13 700 M^{-1} cm^{-1}; G = 11 700 M^{-1} cm^{-1}). All experiments were carried out in 100 mM NaCl, 10 mM sodium phosphate buffer (pH = 7.0), and 0.1 mM EDTA. The cyanine dye *N*,*N*′-diethylthiadicarbocyanine iodide DiSC2(5) (see Figure 2) was purchased from Molecular Probes, Inc (Eugene, OR) and used as received. Molecular Probes no longer sells this dye, but it can be purchased from Aldrich Chemical Co. (Milwaukee, WI). Stock solutions of the dye were prepared in methanol and filtered through glass wool. Concentrations were determined spectrophotometrically using ϵ_{651} = 260 000 M^{-1} cm^{-1} in methanol.

Hybridization Studies. The appropriate single strands were hybridized by the following procedure: Samples were heated to 95 °C and then cooled at a rate of 1 °C/min while monitoring the ABS (absorbance hypochromicity) or CD (circular dichroism) signals at 275 nm with a data interval of 0.5 °C. Subsequent reheating under the same conditions revealed no hysteresis effect.

Circular Dichroism. CD experiments were performed on a Jasco J-715 spectrophotometer. All spectra represent an average of at least eight scans and were collected at a rate of 100 nm/min. All spectra are baseline subtracted and if necessary smoothed via (at most) a five point adjacent averaging algorithm. PNA−DNA hybrids were prepared either by mixing the two strands and incubating at room temperature for 15 min or by heating to 95 °C followed by slow cooling to 20 °C prior to recording spectra. The two methods yielded similar spectra; data shown in the figures were collected on heat−cool annealed samples.

Evaluation of Melting Curves. The absorbance at 275 nm was plotted versus the temperature and fit to a two-state model of the hybridization. The thermodynamic parameters ΔH and ΔS are assumed to be temperature independent, and the heat capacity is assumed to remain constant throughout the processes.[59]

The equilibrium constant for both the duplex to single-strand transition and the hairpin to random-coil transition is expressed as

$$K = \frac{\alpha(C_t/n)}{[(1-\alpha)C_t/n]^n} \tag{1}$$

where C_t is the total strand concentration, n is the molecularity of the process, and α is the fraction of single strands in a duplex or hairpin state, respectively. Melting data are plotted as $(1 - \alpha)$ versus temperature. The α parameter is calculated by determining an upper (x) and lower (y) baseline for the melting transition, and calculating α at each temperature as

$$\alpha = 1 - \frac{\text{abs} - y}{x - y} \tag{2}$$

The Van't Hoff expression in these terms is[59]

$$\Delta H_{VH} = (2 + 2n)RT_m^2\left(\frac{d\alpha}{dT}\right)_{T=T_m} \tag{3}$$

where ΔH_{VH} is the van't Hoff enthalpy and R is the ideal gas constant.

ΔH and ΔS values were also obtained via a more rigorous concentration dependent analysis, where $1/T_m$ of a given duplex is plotted against the total strand concentration. The slope of such a plot is proportional to the enthalpy of the process, and the Y-intercept is proportional to the entropy:[59]

$$\underset{(y)}{\frac{1}{T_m}} = \underset{(m)}{\frac{(n-1)R}{\Delta H}} \underset{(x)}{\ln C_t} + \underset{(b)}{\frac{[\Delta S^\circ - (n-1)R\ln 2n]}{\Delta H}} \tag{4}$$

Comparison of both the shape and concentration dependent methods of analysis yielded thermodynamic parameters that were in all cases within 10% of each other, indicating that the two-state approximation is valid.

In cases where the T_m values of the probe−target duplex and of the target hairpin were sufficiently close to preclude defining the upper baseline of the former transition, a subtraction method was used to isolate the probe−target transition. In this procedure, three samples were prepared containing (A) 5.0 μM probe alone, (B) 5.0 μM target alone, and (C) 5.0 μM each probe and target together. Melting curves were recorded for the three samples, and then the sum of A and B was subtracted from C. This procedure is illustrated for hybridization of the two hairpins **T4** and **P10** in Figure S6 (Supporting Information). The resulting curve was analyzed by the methods described above to determine the T_m and thermodynamic parameters.

Colorimetric Detection of Hybridization. Samples were prepared containing 5.0 μM of **T1** and **P1**, separately or in combination, in 10 mM sodium phosphate buffer (pH = 7.0) with 10% methanol to prevent adsorption of the dye to the cuvette. After mixing the components, baseline absorption spectra were recorded at 15 °C from 450 to 750 nm. 5.0 μM DiSC2(5) was then added to the cuvettes, and spectra were acquired at 15 °C. (The lower temperature is required to allow the dye to bind to the duplex.)

Kinetic Analysis. The rate of duplex formation was measured, under constant mixing, in the following manner: A cuvette containing the target strand was incubated at 25 °C. The probe strand was then added to the target strand with a dead time of less than 5 s. The absorbance of the sample was monitored at 275 nm until there was no appreciable change of absorbance with time. Results were analyzed via a 2nd order fitting equation. Initial estimates for the absorbance at $t = 0$ were determined by the concentrations of the oligonucleotides that were used. Strand concentrations were 15 μM each in these experiments. The higher concentrations were used to enhance the signal/noise ratio in the data, because $\Delta A_{275} = 0.3$, versus 0.1 for the lower strand concentrations used for the thermal denaturation experiments.

Results

Target Selection. To begin our studies of the effects of target structure on PNA hybridization, we selected DNA hairpins based on the GAAA tetraloop motif. The prevalence of GAAA containing sequences near replication origins and promoters suggests a potential biological relevance for these sequences.[60,61]

(57) Morrison, W. R. *Anal. Biochem.* **1964**, *7*, 218−224.
(58) Christensen, L.; Fitzpatrick, R.; Gildea, B.; Petersen, K. H.; Hansen, H. F.; Koch, T.; Egholm, M.; Buchardt, O.; Nielsen, P. E.; Coull, J.; Berg, R. H. *J. Pept. Sci.* **1995**, *3*, 175−183.
(59) Marky, L. A.; Breslauer, K. J. *Biopolymers* **1987**, *26*, 1601−1620.

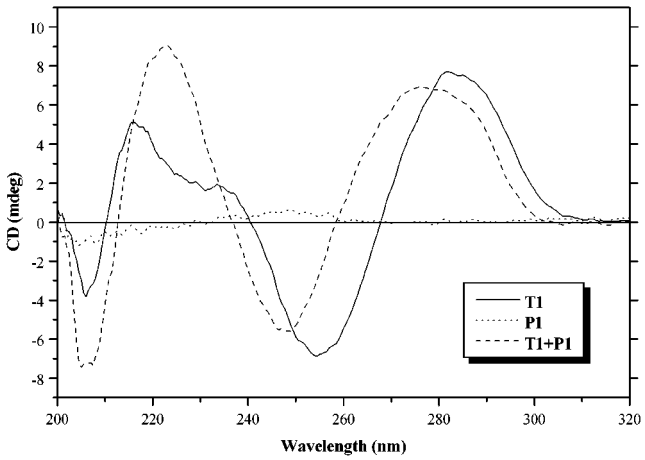

Figure 1. CD spectra of 5 μM **T1**, 5 μM **P1**, and 5 μM **T1** annealed to 5 μM **P1** in 10 mM NaP_i (pH = 7.0), 100 mM NaCl, and 0.1 mM EDTA. All spectra were measured at 20 °C and represent the average of eight scans collected at 100 nm/min.

Regardless of the biological importance of this motif, the GAAA tetraloop represents a challenging target for a hybridization probe based on the extremely high stability of even the shortest members of this family. For example, the sequence 5′-*GC*GAAA*GC*-3′ folds into a hairpin consisting of the GAAA loop and a two base pair (bp) stem. (Nucleotides that form the stem are italicized.) The hairpin is surprisingly stable to thermal denaturation, only unfolding to a random coil state at ∼76 °C.[26] The stability is believed to arise from formation of a sheared G−A pair between G3 and A6 and stacking of A4 and A5 on top of A6 within the loop.[62,63] Extending the stem of the hairpin leads to corresponding increases in stability for the hairpin. The sequences and secondary structures of all target and probe molecules used in this study are shown in Chart 1.

Hairpin Invasion by PNA. Figure 1 presents circular dichroism (CD) spectra recorded for **P1**, **T1**, and **P1** + **T1**. The spectrum for the 1:1 mixture of the DNA target and the PNA probe is clearly not simply the sum of the two component strands, reflecting interaction between the two components. The extrema observed for the mixture, namely maxima at 223 and 280 nm and a minimum at 248 nm, are characteristic of PNA−DNA duplexes,[33] indicating successful hybridization of the PNA to its target. Similar spectra were obtained for 1:1 mixtures of **P1** with **T2** and **T3** (Figure S1, Supporting Information). It is important to note that these duplexes form spontaneously at room temperature, even though the hairpins have melting temperatures ranging from 76 to 90 °C.

Formation of the PNA−DNA hybrid was also monitored using the cyanine dye DiSC2(5) (Figure 2) which we previously reported as the first high-affinity ligand and colorimetric indicator for PNA-containing hybrids.[64] The absorption spectrum of the dye is shifted by ∼120 nm in the presence of PNA-containing duplexes or triplexes, but not when PNA is unhybridized. Figure 2 shows UV−vis absorption spectra recorded for DiSC2(5) in the presence of **P1**, **T1**, and **P1** + **T1**. The

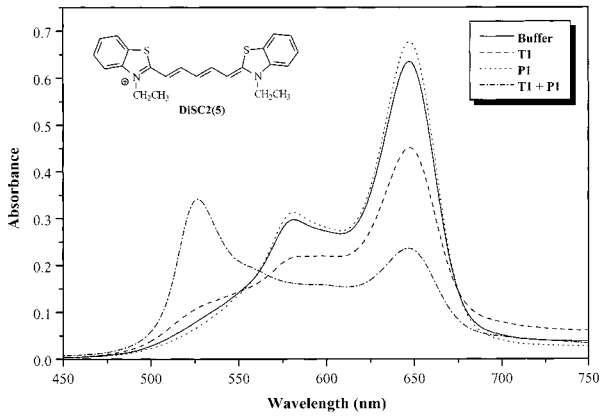

Figure 2. UV−vis spectra of 5 μM **DiSC2(5)** in the presence of buffer (10 mM NaP_i, 10% MeOH), 5 μM **T1**, 5 μM **P1**, and 5 μM annealed **T1**−**P1** duplex. All spectra were collected at 15 °C.

unbound dye shows a maximum at 650 nm, and this is the dominant peak for the two isolated components. However, in the 1:1 mixture, a new band at 530 nm is observed, indicative of successful hybridization.

Thermodynamics of Hairpin Invasion. The circular dichroism and colorimetric indicator experiments demonstrate that the PNA probe successfully disrupts the stable secondary structure of the DNA targets, constituting a "hairpin invasion" process. These qualitative experiments do not provide any insight into the thermodynamics or kinetics of the process. The thermodynamics of hybridization events can be analyzed using optical melting curves, in which the absorbance at a single wavelength is monitored as a function of temperature. Nucleic acid structural transitions are most often detected by UV absorbance at 260 nm (A_{260}).[65] However, observation of melting transitions at other wavelengths can often improve signals or detect otherwise invisible transitions.[66] In the selected sequences, there is a large percentage of G and C bases, and the absorbance spectra for these bases (in particular cytosine) shifts the maximum absorbance toward 280 nm.[65] Hence, we monitored hybridization and denaturation processes at 275 nm. Curve-fitting procedures and concentration-dependent analyses can be used to extract the free energy, enthalpy, and entropy of hybridization.[59] We hoped to characterize the thermodynamics of the hairpin−coil transition for **T1**, but two effects prevented this: (1) the high denaturation ("melting") temperature for the transition made it difficult to obtain a distinct upper baseline, which is needed for effective curve-fitting according to the method of Marky and Breslauer;[59] and (2) the short two bp stem leads to a relatively low cooperativity of melting, which is manifested as a broad transition. To counteract this, we redesigned the sequence to yield a more cooperative transition without increasing the melting temperature. Thus, two additional base pairs were added to the stem, but the sequence of bases within the stem was altered to give **T4**: 5′-*CGCG*GAAA*CGCG*-3′. Inverting the closing base pair from C−G to G−C has been shown to substantially destabilize the hairpin structure and, thus, compensate for the extended stem.[9] Thus, the melting temperature for **T4** is 75.5 °C, virtually identical to that of **T1**. Moreover, the transition temperature is independent of DNA concentration over the range 1−20 μM, as expected for a unimolecular process.

(60) Cotmore, S. F.; Tattersall, P. *EMBO J.* **1994**, *13*, 4145−4152.
(61) Chung, H. Y.; Hong, M. H.; Chun, Y. H.; Bai, S.; Im, S. Y.; Lee, H. B.; Park, J. C.; Kim, D. H.; Chun, S. B. *J. Microbiol. Biotechnol.* **1998**, *8*, 650−655.
(62) Yoshizawa, S.; Kawai, G.; Watanabe, K.; Miura, K.-i.; Hirao, I. *Biochemistry* **1997**, *36*, 4761−4767.
(63) Menger, M.; Eckstein, F.; Porschke, D. *Biochemistry* **2000**, *39*, 4500−4507.
(64) Smith, J. O.; Olson, D. A.; Armitage, B. A. *J. Am. Chem. Soc.* **1999**, *121*, 2686−2695.
(65) Blackburn, G. M.; Gait, M. J. *Nucleic Acids in Chemistry and Biology*, 2nd ed.; Blackburn, G. M., Gait, M. J., Eds.; Oxford University Press: New York, 1996.
(66) Davis, T. M.; McFail-Isom, L.; Keane, E.; Williams, L. D. *Biochemistry* **1998**, *37*, 6975−6978.

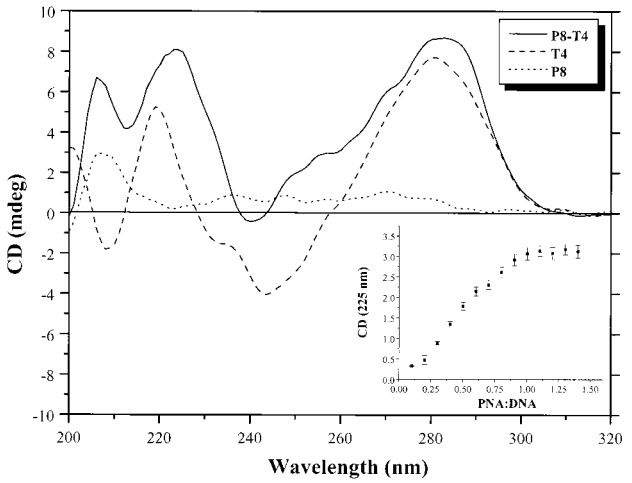

Figure 3. CD spectra of 10 μM **T4**, 10 μM **P8**, and 10 μM **T4** annealed to 10 μM **P8**. All spectra were measured at 20 °C and represent the average of 10 scans collected at 100 nm/min. Inset: Titration of **P8** into 10 μM **T4** monitored by CD at 225 nm.

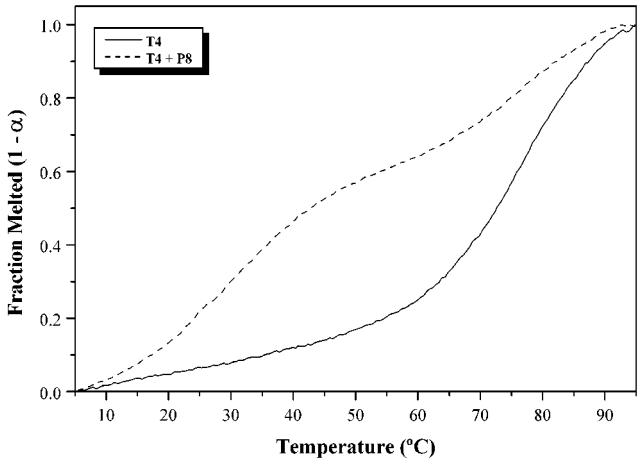

Figure 4. Fraction melted (1 − α) monitored at 275 nm for 10 μM **T4** (solid line), and 10 μM **T4** + 10 μM **P8** (dashed line). Data were collected every 0.5 °C during a heating ramp of 1 °C/minute (no hysteresis was observed when compared to the cooling ramps).

PNA probes complementary to the central 8 or 10 bases of **T4** were synthesized (**P8** and **P10**, Chart 1). CD analysis of **P8** + **T4** revealed successful hybridization (Figure 3) and a titration experiment was consistent with a 1:1 stoichiometry for the hybrid (Figure 3 inset). Thermal denaturation experiments were then performed by monitoring the UV absorbance at 275 nm as a function of temperature. Figure 4 illustrates melting curves recorded for **T4** alone and in the presence of **P8**. The higher temperature transition occurs at 75.5 °C in both cases and is assigned to the hairpin−coil transition of the DNA target. The lower temperature transition is concentration-dependent, however, varying from 22.0 to 31.8 °C over the range 3−20 μM total strand concentration. This is consistent with a bimolecular process.

Thermodynamic parameters for the hairpin−coil transition of **T4** alone and for the duplex melting process of the **T4**−**P8** hybrid were obtained through the established curve-fitting procedure originally developed by Marky and Breslauer (Table 1).[59] Both transitions are enthalpically driven, with negative ΔH and ΔS terms. The duplex denaturation transition was also analyzed using the concentration dependence of the melting temperature, and the thermodynamic parameters obtained by this method agreed with those from the curve-fitting procedure to within 10%, indicating that the melting process was essentially a two-state transition.[59]

Table 1. Thermal and Thermodynamic Parameters for Hairpin Invasion by PNA Probes[a]

structure	T_m (°C)	$-\Delta G_{(298\ K)}$	$-\Delta H$	$-T\Delta S_{(298\ K)}$
T4	75.5 ± 0.5	4.8 ± 1.5	33.5 ± 0.8	28.7 ± 0.7
T4−**P8**	24.8 ± 1.1	8.0 ± 3.7	40.3 ± 2.0	32.3 ± 1.7
T4−**P10**	46.8 ± 0.7	11.2 ± 2.3	46.0 ± 1.3	34.8 ± 1.0

[a] T_m values reported are at 5 μM total strand concentration. Thermodynamic values given in kcal/mol.

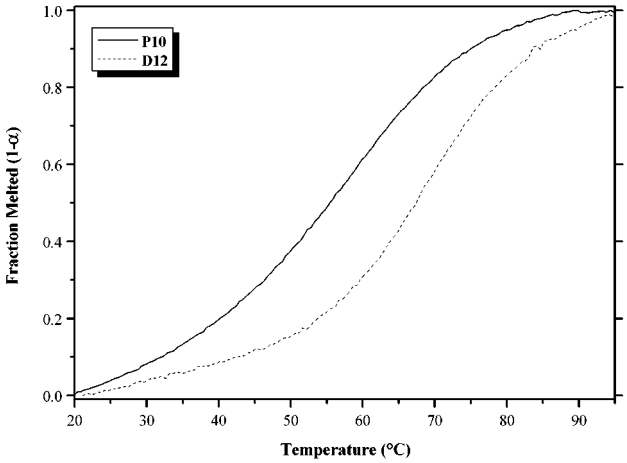

Figure 5. Fraction melted (1 − α) monitored at 275 nm for 10 μM **P10 (**solid line), and 10 μM **D12** (dotted line). Data were collected every 0.5 °C during a heating ramp of 1 °C/minute.

Hairpin invasion by the extended probe **P10** was studied next. Thermal denaturation experiments demonstrated that **P10** successfully disrupted the **T4** hairpin to form a duplex with T_m = 46.8 °C and ΔG = −11.2 kcal/mol (Table 1). Thus, the **T4**−**P10** duplex exhibits greater thermal and thermodynamic stability than the corresponding **T4**−**P8** duplex (ΔT_m = 22 °C and $\Delta\Delta G$ = −3.2 kcal/mol), as expected, because **T4**−**P10** has two additional base pairs. Another interesting result from the experiments using **P10** was the presence of secondary structure in the unhybridized PNA probe. A thermal denaturation experiment on **P10** alone revealed a cooperative melting transition with T_m = 56.3 °C and ΔG = −1.8 kcal/mol (Figure 5). The melting temperature is ∼15 °C higher than the well-known unfolding temperature of single-stranded PNA.[67] On the basis of the sequence, we tentatively assign this structure to a hairpin with a four base loop and three base pair stem. However, a CD spectrum of **P10** alone was very weak and offered no definitive evidence for this structure. Nevertheless, a PNA hairpin with a 5 base loop and 7 bp stem has been reported previously.[23] Regardless of the actual structure of the probe, hybridization of **P10** and **T4** at room temperature requires the disruption of two stable secondary structures.

To provide a context for the experiments with the hairpin target **T4**, we also analyzed hybridization of **P8** with three unstructured targets, **T5, T6**, and **T7** (Chart 1). Each of these targets has the same 8 base recognition sequence as **T4** but differs in its flanking region. **T5** is a truncation analogue in which the last two nucleotides on both ends of the sequence have been deleted. This corresponds to eliminating the last two base pairs from the stem of **T4**, which destabilizes the hairpin structure and leads to a duplex in which the PNA and DNA

(67) Nielsen, P. E.; Egholm, M. *Peptide Nucleic Acids. Protocols and Applications*; Nielsen, P. E., Egholm, M., Eds.; Horizon Scientific Press: Norfolk, 1999.

Table 2. Thermal and Thermodynamic Parameters for Hybridization of PNA Probe P8 with DNA Targets T4−T7[a]

target	T_m (°C)	$-\Delta G_{(298\ K)}$	$-\Delta H$	$-T\Delta S_{(298\ K)}$
T4	24.8 ± 1.1	8.0 ± 3.7	40.3 ± 2.0	32.3 ± 1.7
T5	34.5 ± 0.8	10.1 ± 3.1	61.2 ± 1.6	51.1 ± 1.5
T6	42.5 ± 0.6	10.8 ± 3.4	48.7 ± 1.8	38.0 ± 1.6
T7	41.5 ± 0.7	10.6 ± 3.2	48.8 ± 1.7	38.1 ± 1.5

[a] T_m values reported are at 5 μM total strand concentration. Thermodynamic values given in kcal/mol.

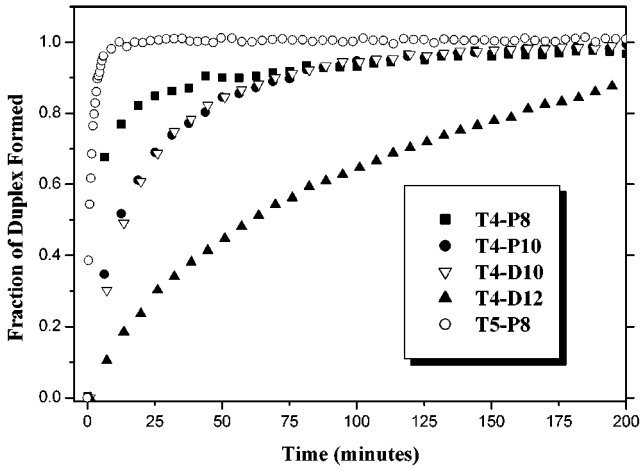

Figure 6. Kinetics of PNA−DNA and DNA−DNA duplex formation as monitored by UV absorbance at 275 nm. All data were collected at 25 °C with a strand concentration of 15 μM each in both target and probe.

strands have the same length. **T6** and **T7** have the same length as **T4**, but the last two nucleotides on each end are scrambled so that, in a hairpin motif, the last two base pairs in the stem would be mismatches. Hybridization of these targets with **P8** produces a duplex with two base overhangs on the DNA strand at both ends. None of these three target sequences exhibit a self-melting transition (data not shown) and, therefore, most likely do not form a hairpin structure over the 10−90 °C range.

Hybridization of **P8** with the three unstructured targets yields PNA−DNA hybrids that are more stable, thermally and thermodynamically, than the **T4**−**P8** duplex (Table 2). For the truncated target **T5**, the T_m increased by 10 °C and ΔG decreased by 2.1 kcal/mol. Even larger stabilizations were observed for the scrambled targets **T6** and **T7**, where ΔT_m = 17−18 °C and $\Delta\Delta G = -2.6-2.8$ kcal/mol. These results clearly demonstrate the negative impact of target structure on PNA hybridization. In each case, the more favorable ΔG for hybridization of PNA to unstructured targets can be traced to the enthalpy change being greater, because there is a larger entropic penalty for the unstructured targets (vide infra).

Kinetics of Hairpin Invasion. The kinetics of hairpin invasion by the PNA probes were analyzed by monitoring the UV absorbance at 275 nm as a function of time after mixing with the DNA target. Hybridization of short oligonucleotides usually requires data collection with stopped-flow instrumentation because of millisecond time scale reactions.[68] However, the introduction of a stable secondary structure into the target sufficiently decreases the rate of hybridization to permit analysis in a conventional UV−vis spectrophotometer. Figure 6 illustrates the results obtained for hybridization of **T4**−**P8**, **T4**−**P10**, and **T5**−**P8**. Hybridization by the two unstructured strands, **P8** and **T5**, occurs the fastest, followed by the unstructured **P8** + structured **T4**, and then followed by the two structured strands, **P10** and **T4**. Quantitatively, introduction of structure into the DNA target reduces the rate of hybridization by a factor of 5, while the folded structure of **P10** retards hybridization by an additional factor of 4 (Table 3). Thus, the higher affinity of the longer probe for the target comes at the cost of slower hybridization kinetics. Doubling the concentration of either the PNA probe or DNA target in these experiments leads to a doubling of the reaction rate, indicative of a reaction that is first-order in both components (data not shown). In addition, measurement of the kinetics at different temperatures permitted determination of the activation energies from Arrhenius plots (Figure S2, Supporting Information). The secondary structure in **P10** increases the activation energy by nearly 50% relative to the unstructured probe **P8** (Table 3).

(68) Turner, D. H.; Sugimoto, N.; Freier, S. M. *Nucleic Acids*; Springer-Verlag: Berlin, 1990; Vol. C.

Table 3. Hybridization Kinetics and Activation Energies for PNA and DNA Probes[a]

duplex	k (1/min·mol)	relative rate	E_a (kcal/mol)
T5−**P8**	$(1.0 \pm 0.2) \times 10^5$	1.0	
T4−**P8**	$(2.0 \pm 0.3) \times 10^4$	0.2	23.9
T4−**P10**	$(4.8 \pm 0.2) \times 10^3$	0.05	34.8
T4−**D10**	$(5.7 \pm 0.2) \times 10^3$	0.06	26.1
T4−**D12**	$(6.0 \pm 0.2) \times 10^2$	0.006	41.0

[a] Conditions: 15 μM in each strand, T = 25 °C.

Table 4. Thermal and Thermodynamic Parameters for DNA−DNA Hybrids[a]

structure	T_m (°C)	$-\Delta G_{(298\ K)}$	$-\Delta H$	$-T\Delta S_{(298\ K)}$
T4−**D10**	42.7 ± 0.6	10.6 ± 2.7	54.6 ± 1.5	44.0 ± 1.2
T4−**D12**	47.1 ± 0.5	12.1 ± 2.7	57.4 ± 1.5	45.3 ± 1.2
M1−**M2**	59.8 ± 0.5	16.6 ± 4.4	89.6 ± 2.3	73.0 ± 2.1

[a] T_m values reported are at 5 μM total strand concentration. Thermodynamic values given in kcal/mol.

Hairpin Invasion by DNA Probes. To provide a comparison with our results using PNA probes, we studied hairpin invasion by three DNA probes, **D8**, **D10**, and **D12**. **D8**, which is analogous to **P8**, did not form a stable hybrid with **T4**, according to thermal denaturation experiments. This indicates that if hybridization were to occur, the **T4**−**D8** duplex would denature at T < 10 °C. This is not a particularly surprising result, given the low T_m of **T4**−**P8**. **D10** and **D12**, on the other hand, successfully disrupted the hairpin structure of the target and formed stable duplexes (Table 4). A number of interesting observations arose from these experiments. First, while there was a significant increase in both the thermal and thermodynamic stabilities for **D10** versus **D8**, **D12** offered only a minor enhancement in stability, considering the experimental error. Second, **D12** adopts a stable secondary structure as monitored by UV melting analysis (Figure 5; concentration-independent T_m = 66.8 °C and $\Delta G = -3.6$ kcal/mol). The CD spectrum of **D12** shows a maximum at 281 nm and minima at 250 and 210 nm (Figure S3, Supporting Information). These signals are qualitatively different from the signals generated by hairpins of the GAAA tetraloop motif.[26] Unfortunately, CD spectra for TTTC tetraloop motifs are not present in the literature for comparison. On the basis of the sequence of **D12**, we tentatively assign the structure observed as a hairpin (Chart 1), whereas **D10** is unstructured under the experimental conditions. Finally, as we observed when comparing **T4**−**P8** and **T5**−**P8** duplexes, the duplex formed from unstructured strands **M1** and **M2** exhibits greater thermal and thermodynamic stability than the **T4**−**D12** duplex (ΔT_m = 12.7 °C; $\Delta\Delta G = -4.5$ kcal/mol). These two duplexes have similar base compositions and predicted T_m's (within 4 °C) based on nearest-neighbor analy-

Scheme 1. Three Types of Hybridization Reactions Studied

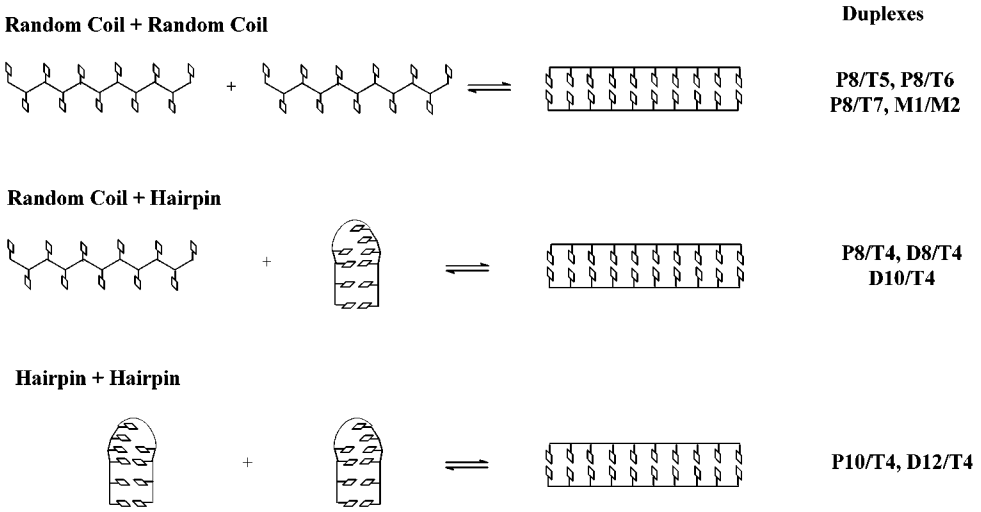

sis,[69,70] so the difference in stabilities is most likely due to the difference in structure for the unhybridized components. A summary of the relevant equilibria for the range of targets and probes can be found in Scheme 1.

Kinetic analysis of the **T4**−**D12** duplex reveals the slowest hybridization kinetics (Figure 6) and largest activation energy of all duplexes studied (Table 3). Duplex formation by **D12** is ∼10-fold slower than for **D10** and is not complete under these conditions after a period of over 3 h. An Arrhenius plot indicates that the secondary structure in **D12** increases the activation barrier by greater than 50% relative to **D10**. Thus, as observed for PNA probes, incorporating structure into the DNA probe leads to significantly slower hybridization.

Discussion

The efficient capture of biological nucleic acids by hybridization probes and effective inhibition of gene expression by antisense and antigene agents require that the hybridization agent successfully overcomes the innate secondary and tertiary structure in the target to gain access to the complementary sequences. While it is widely believed that the presence of such structure in the target will impose thermodynamic and kinetic barriers to hybridization, few quantitative studies of these effects have been reported. The kinetic barrier associated with the hybridization of structured targets has been associated with reduction in antisense efficacy.[71] Structure present in complementary strands has been shown to reduce the thermodynamic stability of the duplex formed[22] but has also been associated with increases in probe−target specificity (i.e., mismatches have a larger effect in a system bearing structure).[25] Thus, we performed the series of experiments described above in which PNA and DNA probes were targeted to stable DNA hairpin targets. The results allow us not only to evaluate the effects of target structure, but also to probe structure, on hybridization thermodynamics and kinetics.

Hybridization to Structured Targets. The **T4** target is an extraordinarily stable hairpin (T_m = 75.5 °C; $\Delta G = -5.5$ kcal/mol) consisting of a four base pair stem and a highly structured four base loop. The 8-mer PNA probe **P8** targets the central 8 nucleotides of the **T4** sequence, meaning successful hybridization produces an 8 bp PNA−DNA duplex with two base DNA overhangs on each end. CD and UV spectroscopy indicate successful hybridization of **P8** to **T4**, and thermodynamic analysis reveals that duplex formation is an enthalpically driven process. It is noteworthy that the T_m of the **T4**−**P8** duplex is ∼50 °C lower than the **T4** hairpin's T_m, yet the PNA successfully disrupts the hairpin secondary structure to gain access to the complementary primary structure. Likewise, the extended **P10** probe overcomes a 29 °C difference in T_m to hybridize with **T4**. The latter case is all the more impressive given that the **P10** probe is itself structured, most likely as a hairpin. This phenomenon can only arise if the free energies of the different structures, namely the hairpin reactants and PNA−DNA duplex product, have significantly different temperature dependencies. This is, in fact, the case, as shown in Figure 7, where the free energies for the **T4** hairpin + **P10** probe and **T4**−**P10** duplex are plotted versus temperature. The solid and dashed lines in the figure were calculated using the equation $\Delta G = \Delta H - T\Delta S$ and the values for the enthalpy and entropy changes determined by thermal denaturation analysis. At temperatures below the **T4**−**P10** melting temperature, the duplex has a lower ΔG than the isolated probe and target. However, above this temperature

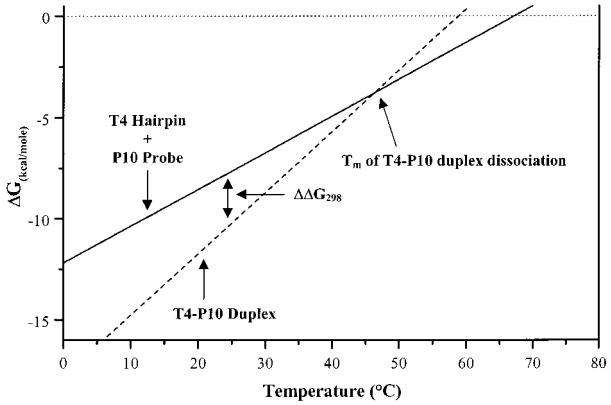

Figure 7. Phase diagram showing the free energies of **T4** + **P10** (two hairpins; solid line) and **T4**−**P10** (duplex; dashed line) plotted as a function of temperature. Free energies were calculated at each temperature using ΔH and ΔS values determined from melting curves. The T_m of duplex dissociation shown by the phase diagram is 46.5 °C relative to the experimental result of 46.8 °C, and the $\Delta\Delta G_{298}$ between the two states is indicated.

(69) Breslauer, K. J.; Frank, R.; Blocker, H.; Marky, L. A. *Proc. Natl. Acad. Sci. U.S.A.* **1986**, *83*, 3746−3750.
(70) Sugimoto, N.; Nakano, S.; Yoneyama, M.; Honda, K. *Nucleic Acids Res.* **1996**, *24*, 4501−4505.
(71) Sohail, M.; Southern, E. M. *Adv. Drug Delivery Rev.* **2000**, *44*, 23−34.

(because of the entropy contribution), there is insufficient binding free energy to allow formation of a stable hybrid.

The free energy of hybridization can be subdivided into enthalpic and entropic contributions. For duplex formation to occur spontaneously, the duplex must lie lower in energy (ΔG) than the hairpin. Because the **T4**−**P10** duplex should have more base pairs and base stacking interactions than the isolated **T4** and **P10** hairpins, the enthalpy term will favor duplex formation. Thus, at lower temperatures, where enthalpic contributions dominate, formation of the **T4**−**P10** duplex occurs spontaneously. At higher temperatures, the entropy term can make significant contributions to the free energy change, because hybridization imposes a loss of translational mobility.[72] The conformational mobility is also likely restricted by hybridization, although this contribution may be muted by the presence of the stable secondary structures in the DNA target and PNA probe. Nevertheless, we anticipate an unfavorable entropy of hybridization, and this is borne out by the data, which demonstrate negative entropy changes for all hybridization reactions studied. Thus, hybridization is no longer a spontaneous process once the temperature exceeds the T_m of the hybrid. This example demonstrates the often neglected fact that thermal stability does not necessarily correlate with thermodynamic stability.[35]

To determine the effect of structure on the hybridization of **P8** to its target, we also selected a structureless target (**T5**) for binding studies. Thermodynamic analysis of the **T5**−**P8** duplex indicated that it was significantly more stable than the **T4**−**P8** duplex ($\Delta T_m = 9.7$ °C; $\Delta\Delta G = -2.1$ kcal/mol). There are two changes in **T5** versus **T4**: the loss of secondary structure in the target and the shorter sequence of **T5** which leads to elimination of the two base overhangs that are positioned on the termini of the **T4**−**P8** duplex. Other results from our lab indicate that DNA overhangs can substantially increase the thermal stability of PNA/DNA duplexes, even for sequences where no such effect is observed for analogous DNA/DNA duplexes.[73] To account for this, we designed targets **T6** and **T7**, which yield hybrids with **P8** that have two base overhangs, as in the case of **T4**, but contained no secondary structure. The **T6**−**P8** and **T7**−**P8** duplexes were more stable than both the **T4**−**P8** and **T5**−**P8** duplexes. The enhanced stability relative to **T5**−**P8** can be traced to the overhanging bases on the DNA strand, while the added enhancement relative to **T4**−**P8** is attributed to the lack of secondary structure in the **T6** and **T7** targets. Thus, **P8** pays a penalty of ∼2.6−2.8 kcal/mol of binding energy in order to overcome the hairpin structure of **T4**. This is consistent with previous work by Breslauer and coworkers who studied a self-structured DNA system. It was shown that strands that have a capacity for self-structure reduce the thermodynamic stability of the duplex that they form.[22] However, the thermal stability of the single-stranded structures was lower than that of the duplex, and so the competing structures were not present at the temperature of duplex dissociation, meaning there was no perturbation of the duplex thermal stability. Our case exhibits a more pronounced effect where both the thermal and thermodynamic stability of the duplex is decreased. Thus, depending on the type of application, the effect of secondary structure could vary. In diagnostics, for instance, thermal stability is often the decisive parameter, while in biological experiments such as antisense applications, binding affinity (at 37 °C) and thus free energy is crucial for activity.

In comparing the kinetics of duplex formation for **T4**−**P8** and **T5**−**P8**, we found that the **T4**−**P8** duplex formed five times more slowly (Table 3). The rate determined for the formation of the **T5**−**P8** duplex is almost identical to previous studies of PNA/DNA duplex formation where only a very small activation barrier was present.[74] We cannot say if the initial "nucleation" event leading to hybridization of **P8** with **T4** involves recognition of the loop bases or the terminal bases of the stem. At first glance, the loop might seem a more likely target. However, the termini of short duplexes are known to "fray" quite readily, meaning that the closing base pair opens and closes rapidly.[75] In addition, the GAAA loop is highly structured and may, in fact, be less accessible than the terminal bases.[76−78] Further experiments with a less structured loop and/or mismatches at the stem terminus might help resolve this issue. Regardless, our results demonstrate quantitatively that the presence of secondary structure leads to decreased hybridization rates

Effect of Probe Structure. The 10-mer PNA **P10** was also studied for hybridization to **T4**. Unlike **P8**, **P10** folds into a stable secondary structure with $T_m = 56.3$ °C and $\Delta G = -3.8$ kcal/mol. This transition was reasonably cooperative and occurred at a higher temperature than the self-melts commonly exhibited by PNA.[79] On the basis of the sequence of the PNA, this structure is most likely a hairpin with a four base loop and a three bp stem. However, the lack of a distinct CD spectrum prevents definitive assignment of the structure. We find that the addition of two base pairs, relative to the **T4**−**P8** duplex, yields a large improvement in duplex stability for **T4**−**P10** ($\Delta T_m = 22$ °C; $\Delta\Delta G = -3.2$ kcal/mol). We also observe that the rate of duplex formation for the **T4**−**P10** duplex is four times slower than for the **T4**−**P8** duplex (Table 3). This rate reduction is expected because of the self-structure found in **P10**. It is interesting to note that the rate of duplex formation is decreased while the thermodynamic stability of the duplex is increased. This implies that the dissociation rate is significantly slower for **T4**−**P10** than for **T4**−**P8**, as expected on the basis of the additional two base pairs present in the duplex.

Comparison with DNA Probes. The results described above are consistent with the conclusion that secondary structure in the probe and/or the target leads to decreases in duplex stability. The higher affinity for unstructured targets typically exhibited by PNA probes relative to DNA is well-documented, and our results indicate that this carries over to structured targets. Thus, while **P8** spontaneously disrupted the **T4** hairpin to hybridize at low temperatures, DNA probe **D8** was incapable of hybridization with this target. The **D10** probe, on the other hand, formed a stable duplex with **T4**. The additional two base pairs evidently provide sufficient enthalpic stabilization to overcome the entropic loss of hybridization. Interestingly, the stability of this duplex is comparable to the **T4**−**P10** duplex. The higher affinity normally exhibited by PNA is offset in this case by the ability of the **P10** probe to fold into a hairpin, reducing the overall free energy of hybridization.

The self-melting analysis of the **D12** probe yielded a transition similar to those of extraordinarily stable hairpins ($T_m = 66.8$

(72) Kool, E. T. *Chem. Rev.* **1997**, *97*, 1473−1487.
(73) Datta, B.; Armitage, B. A. *J. Am. Chem. Soc.* **2001**, *123*, 9612−9619.
(74) Aich, P.; Nielsen, P.; Rigler, R. *Nucleosides Nucleotides* **1997**, *16*, 609−615.
(75) Nonin, S.; Leroy, J.-L.; Gueron, M. *Biochemistry* **1995**, *34*, 10652−10659.
(76) Pley, H. W.; Flaherty, K. M.; McKay, D. B. *Nature* **1994**, *372*, 111−113.
(77) Butcher, S. E.; Dieckmann, T.; Feigon, J. *EMBO J.* **1997**, *16*, 7490−7499.
(78) Leulliot, N.; Baumruk, V.; Abdelkafi, M.; Turpin, P. Y.; Namane, A.; Gouyette, C.; Huynh-Dinh, T.; Ghomi, M. *Nucleic Acids Res.* **1999**, *27*, 1398−1404.
(79) Tomac, S.; Sarkar, M.; Ratilainen, T.; Wittung, P.; Nielsen, P. E.; Nordén, B.; Gräslund, A. *J. Am. Chem. Soc.* **1996**, *118*, 5544−5552.

Scheme 2. Targeting a Hairpin Asymmetrically to Enhance Hybridization Kinetics

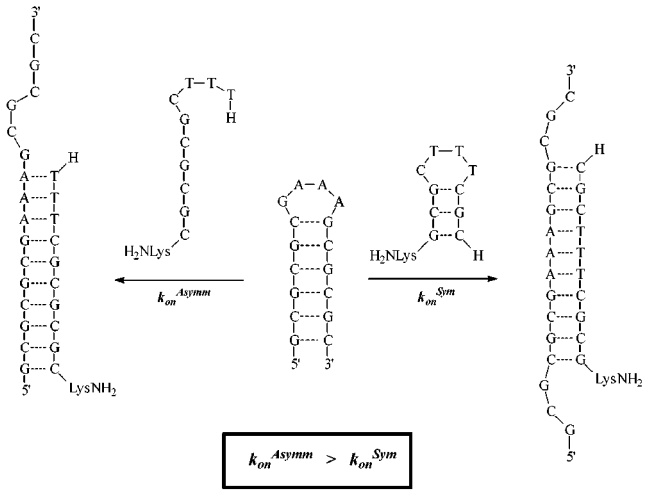

°C; $\Delta G = -3.6$ kcal/mol). The stability of the **D12** secondary structure should not be surprising. If the prevalence of GAAA sequences in critical regions of the genome is biologically significant and leads to extrusion of hairpins from the duplex, it stands to reason that the complementary (TTTC) strand could also form a stable hairpin, yielding a cruciform structure. **D12** was capable of forming a duplex with **T4**, but the duplex was only slightly more stable than the **T4**−**D10** duplex ($\Delta T_m = 4.4$ °C; $\Delta\Delta G = -1.5$ kcal/mol). The self-structure of **D12** likely deteriorates the thermal and thermodynamic stability of the **T4**−**D12** duplex, and hence, the improvement in binding is minimal regardless of the addition of two base pairs. For comparison, we designed two unstructured complementary DNA oligonucleotides (**M1** and **M2**) that bore no self-structure and contained a similar base composition to the **T4**−**D12** duplex. The **M1**−**M2** duplex exhibits substantial improvements in both thermal and thermodynamic stability ($\Delta T_m = 13$ °C; $\Delta\Delta G = -4.5$ kcal/mol). In addition, a nearest-neighbor analysis of the **T4**−**D12** duplex yields a predicted T_m of 56 °C,[69,70] which is 9 °C higher than the observed T_m. Thus, by all accounts the stability of the **T4**−**D12** duplex is lower than that predicted for a system where neither the probe nor the target is structured.

The hybridization rate for **T4**−**D10** was only slightly faster than that for **T4**−**P10**. While the unstructured DNA probe should hybridize faster than the structured PNA probe, **D10** and **T4** repel one another electrostatically, likely raising the activation barrier for hybridization. The slowest hybridization rate occurs for probe **D12**. In this case, the probe must overcome both its own structure and Coulombic repulsion in order to hybridize. In summary, the kinetics of duplex formation follow the order **T4**−**D12** < **T4**−**P10** < **T4**−**D10** < **T4**−**P8** < **T5**−**P8**: the least structured strands hybridize the fastest. In general, the rates we observe with structured probes are at least 10 times slower than what would be expected from unstructured systems.[80] Slow kinetics could present significant problems for hybridization probes, and it is common procedure to avoid self-complementarity when designing these for hybridization or PCR reactions. Naturally, probes of hairpins which target a symmetrical region around the hairpin loop, by definition, will be capable of folding into hairpins. In these cases, targeting the hairpin asymmetrically would likely yield a more effective probe (Scheme 2),[21] as previously found in oligonucleotide hybridization to tRNA.[81−83]

Outlook. Our studies illustrate the ability of both PNA and DNA probes to hybridize to DNA hairpins of extraordinary thermal stablility. The presence of structure in both target and probe has been shown to reduce the overall affinity of the probe and the kinetics of hybridization. The targets of hybridization probes may unavoidably bear secondary structure elements that must be overcome for the probe to be effective. We show that even a small secondary structure such as a hairpin can lead to significant decreases in probe affinity and hybridization kinetics. Strategies are currently in use that apply combinatorial methods to generate a library of all possible hybridization agents for a given target, and high throughput screening methods allow for rapid identification of useful hybridization agents.[81,84,85] The proper design and careful secondary structure analysis of both probes and targets may permit rational optimization of antisense agents, as demonstrated for antisense RNA targeted toward HIV-1.[86] However, it is not yet possible to quantitatively predict activity of antisense oligonucleotides based on RNA secondary structure predictions, although qualitative trends can be predicted.[87]

Future studies in our labs will be dedicated to understanding the nature of the kinetic barriers imposed by self-structured strands. In addition, we note that structured probe sequences such as **P10** and **D12** are not necessarily undesirable, because Kramer and co-workers have shown that such probes exhibit greater sensitivity to mismatches than do unstructured probes.[25] However, the kinetic and thermodynamic penalties imposed by the secondary structure of the probe need to be taken into account. Finally, we intend to continue our studies with the probing of more complex structures (such as loop−loop tertiary interactions), with the hope that improved probes can be developed for the regulation of biologically active DNA and RNA.

Acknowledgment. We are grateful to the National Institutes of Health (R01 GM58547-02) for support of this research and to John Cafardi for assistance with preliminary experiments. We thank Prof. W. David Wilson for helpful discussions. Mass spectra were measured in the Center for Molecular Analysis at Carnegie Mellon University, supported by NSF Grant CHE-9808188.

Supporting Information Available: CD spectra of T2 ± P1, T3 ± P1, and D12; thermal denaturation curves and kinetic data with fits for probe−target duplexes. This material is available free of charge via the Internet at http://pubs.acs.org.

JA016310E

(80) Parkhurst, K. M.; Parkhurst, L. J. *Biochemistry* **1995**, *34*, 285−292.

(81) Mir, K. U.; Southern, E. M. *Nat. Biotechnol.* **1999**, *17*, 788−792.

(82) Petyuk, V.; Serikov, R.; Tolstikov, V.; Potapov, V.; Giege, R.; Zenkova, M.; Vlassov, V. *Nucleosides Nucleotides Nucleic Acids* **2000**, *19*, 1145−1158.

(83) Beloglazova, N. G.; Sil'nikov, V. N.; Zenkova, M. A.; Vlassov, V. V. *FEBS Lett.* **2000**, *481*, 277−280.

(84) Mishra, R. K.; LeTinevez, R.; Toulme, J. J. *Proc. Natl. Acad. Sci. U.S.A.* **1996**, *93*, 10679−10685.

(85) LeTinevez, R.; Mishra, R. K.; Toulme, J. J. *Nucleic Acids Res.* **1998**, *26*, 2273−2278.

(86) Patzel, V.; Sczakiel, G. *Nat. Biotechnol.* **1998**, *16*, 64−68.

(87) Vickers, T. A.; Wyatt, J. R.; Freier, S. M. *Nucleic Acids Res.* **2000**, *28*, 1340−1347.